

Virtual-State Spectroscopy with Frequency-Tailored Intense Entangled Beams

J. SVOZILÍK^{1,2,*}, J. PEŘINA JR.², AND R. DE J. LEÓN-MONTIEL³

¹Quantum Optics Laboratory, Universidad de los Andes, A.A. 4976, Bogotá D.C., Colombia

²Joint Laboratory of Optics of Palacký University and Institute of Physics of CAS, Faculty of Science, Palacký University, 17. listopadu 12, 771 46 Olomouc, Czech Republic

³Instituto de Ciencias Nucleares, Universidad Nacional Autónoma de México, Apartado Postal 70-543, 04510 Cd. Mx., México

*jiri.svozilik@gmail.com

In this contribution we analyze virtual-state spectroscopy — a unique tool for extracting information about the virtual states that contribute to the two-photon excitation of an absorbing medium — as implemented by means of intense entangled beams with tunable spectral correlations. We provide a thorough description of all contributing terms (classical and quantum) in the two-photon absorption signal, as well as the limits imposed by the power of the pump that produces the entangled beams on the observability of the spectral lines of the virtual transitions. We find that virtual-state spectroscopy may be implemented with entangled twin beams carrying up to 10^4 photon pairs. This implies that, in principle, one might be able to detect two-photon absorption signals up to four orders of magnitude larger than previously reported, thus paving the way towards the first experimental realization of the virtual-state spectroscopy technique.

1. INTRODUCTION

Nonlinear spectroscopy has become an invaluable tool across many fields of research [1, 2]. In particular, two-photon absorption (TPA) spectroscopy [for the scheme, see Fig. 1] has allowed us to obtain information about a sample that would not be accessible otherwise. Interestingly, the use of entangled light in two-photon spectroscopy has received a great deal of attention very recently [3–20] because of the unique phenomena that arise in the interaction of entangled photon pairs with matter. Examples of these effects are the linear scaling of the TPA rates on the photon flux [21], two-photon-induced transparency [22], the ability to select different states in complex biological aggregates [23], and the control of entanglement in matter [24, 25]. Indeed, the prediction and observation of these fascinating effects can be understood as a direct consequence of the dependence of the TPA signal on the properties of quantum light that interacts with the sample [26].

Among different techniques proposed over the years, entangled-photon virtual-state spectroscopy (VSS) [27–29] has proved to be a unique tool for extracting information about the virtual states — energy non-conserving atomic transitions [30, 31] — that contribute to the two-photon excitation of an absorbing medium. In this technique, virtual-state transitions, a signature of the medium, are experimentally revealed by introducing a time-delay between frequency-correlated photons,

and averaging over experimental realizations differing in temporal correlations between them [27].

One important aspect of VSS is that the overall TPA rate, R , can be expressed as [22]

$$R = \sigma_E \phi + \delta_r \phi^2, \quad (1)$$

where σ_E is the entangled-light absorption cross section, δ_r is the random (classical) TPA cross section, and ϕ is the flux density of photon pairs. Notice that Eq. (1) states that entangled-photon effects will dominate the TPA signal only when the photon-flux density is sufficiently small. This conclusion has two opposite points of view when discussing the experimental implementation of VSS. On one hand, the low efficiency of spontaneous down-conversion in nonlinear crystals guarantees the low photon-flux condition but, on the other, a low photon-flux might result in an extremely weak TPA signal that might require long measuring times, thus making the implementation of virtual-state spectroscopy an unrealistic endeavor.

With the advent of ultrahigh flux sources of entangled photons [32–37], one naturally wonders whether VSS can benefit from them, especially because it has been shown that strong frequency correlations between entangled beams persist at high photon-flux conditions [38–41]. Consequently, in this paper, we provide a thorough analysis of VSS when implemented with intense entangled fields (further twin beams). This allows us to

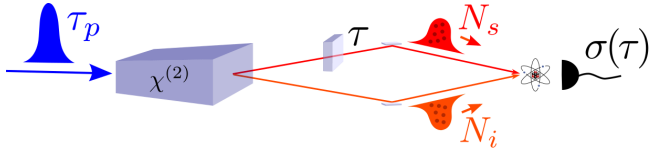


Fig. 1. Schematic representation of the two-photon absorption process caused by two mutually-delayed beams that form a common twin beam. A nonlinear $\chi^{(2)}$ crystal is pumped by an intense laser pulse, thus producing two intense entangled beams. These beams interact with an absorbing medium and the two-photon absorption signal is measured as a function of an externally-introduced delay τ between them; τ_p stands for the pump-pulse duration and $N_{s,i}$ is the number of photons present in the signal and idler beams, respectively.

determine the entangled-photon flux threshold at which spectroscopic information about an absorbing medium can be retrieved. Surprisingly, we find that virtual-state spectroscopy may be implemented with twin beams carrying up to 10^4 photon pairs. This means that the strength of typical TPA signals could be enhanced by up to four orders of magnitude, thus paving the way towards the first experimental realization of virtual-state spectroscopy.

The paper is structured as follows. In Sec. II we describe the generation of twin beams, produced in a nonlinear crystal pumped by an intense laser pulse. In Sec. III, we derive the explicit form of the TPA signal for temporally-delayed intense twin beams. In Sec. IV, we provide an example of the VSS implementation with intense twin beams by extracting the energy level structure of a model system, whose two-photon excitation takes place via three intermediate states with randomly chosen energies. Finally, in Sec. V we present our conclusions.

2. GENERATION OF INTENSE TWIN BEAMS

To describe the generation of twin beams, we follow the procedure used by previous authors in Refs. [38, 39, 42–46]. The first step is to solve the Schrödinger equation in the first-order perturbation approximation to obtain the two-photon spectral amplitude. In the second step the Schmidt decomposition of the two-photon spectral amplitude (TSA) of the generated photons is calculated. This provides the Schmidt modes of the correlated photon fields. The twin-beam description is then found by solving the Heisenberg equations for the creation and annihilation operators of the corresponding Schmidt spectral modes.

Let us start with the description of Spontaneous Parametric Down-conversion (SPDC) in the Schrödinger picture, based on the momentum operator

$$\hat{G}(z) = 4\epsilon_0 A \int_{-\infty}^{\infty} dt \chi^{(2)} \mathcal{E}_p^{(+)}(z, t) \hat{E}_s^{(-)}(z, t) \hat{E}_i^{(-)}(z, t) + \text{h.c.} \quad (2)$$

where ϵ_0 is the vacuum permittivity, A is the traverse area of interaction, $\chi^{(2)}$ is the second-order non-linear susceptibility and h.c. stands for the Hermitian-conjugated term. The pump field is modeled as a classical non-depleted field with the form

$$\mathcal{E}_p^{(+)}(z, t) = \frac{1}{\sqrt{2\pi}} \int_{-\infty}^{\infty} d\omega_p e_p(\omega_p) \exp[-i(\omega_p t - k_{zp} z)]. \quad (3)$$

Notice that the spatial dependence is encapsulated in the longitudinal wave vector k_{zp} . Transversally, we consider the pump

homogeneous in the whole area A . The pump spectrum is given by

$$e_p(\omega_p) = \zeta_p \sqrt{\frac{\tau_p}{\sqrt{2\pi}}} \exp\left[-\frac{\tau_p^2}{4} (\omega_p - \omega_p^0)^2\right]. \quad (4)$$

Here, the pump pulse duration is denoted by τ_p and the pump amplitude is described by $\zeta_p = \sqrt{P_p / \epsilon_0 c f n_p}$, which depends on the pump power P_p and the repetition frequency f ; n_p is the index of refraction of the crystal at the pump wavelength, and c is the speed of light. Finally, the generated signal and idler photons are treated in a quantum manner and they are described by the positive-frequency electric-field operator amplitude

$$\hat{E}_j^{(+)}(z, t) = \frac{i}{\sqrt{2\pi}} \int_{-\infty}^{\infty} d\omega_j \sqrt{\frac{\hbar \omega_j}{2\epsilon_0 A c n_j}} \hat{a}(\omega_j) \times \exp[-i(\omega_j t - k_j z)], \quad (5)$$

with $j = s, i$; \hbar is the reduced Planck constant and $\hat{a}_j(\omega_j)$ is the bosonic annihilation operator of the j th photon with frequency ω_j .

The first-order perturbation solution of the Schrödinger equation results in the following entangled two-photon state

$$|\Phi\rangle = -\frac{i}{\hbar} \int_0^L dz \hat{G}(z) |\text{vac}\rangle = \int_{-\infty}^{\infty} d\omega_s \int_{-\infty}^{\infty} d\omega_i \Phi(\omega_s, \omega_i) \hat{a}_s^\dagger(\omega_s) \hat{a}_i^\dagger(\omega_i) |\text{vac}\rangle, \quad (6)$$

where L stands for the length of the non-linear crystal and $|\text{vac}\rangle$ denotes the vacuum state of the signal and idler fields in front of the crystal. The TSA $\Phi(\omega_s, \omega_i)$ is given by

$$\Phi(\omega_s, \omega_i) = \frac{i\chi^{(2)}\zeta_p L}{\sqrt{2\pi n_p n_s n_i}} \sqrt{\frac{\tau_p}{\sqrt{2\pi}}} \text{sinc}\left[\Delta k_z(\omega_s, \omega_i) \frac{L}{2}\right] \times \exp\left[-\frac{\tau_p^2}{4} (\omega_s + \omega_i - \omega_p^0)^2 - i\Delta k_z(\omega_s, \omega_i) \frac{L}{2}\right] \quad (7)$$

with $\Delta k_z(\omega_s, \omega_i) = k_{zp}(\omega_s + \omega_i) - k_{zs}(\omega_s) - k_{zi}(\omega_i)$.

We now proceed with the second step of the calculation, where the Schmidt decomposition is applied to find pairs of spectral modes [47, 48] of the normalized TSA, that is,

$$\tilde{\Phi}(\omega_s, \omega_i) = \sum_{g=1}^{\infty} \lambda_g f_{s,g}^*(\omega_s) f_{i,g}^*(\omega_i), \quad (8)$$

with $\Phi = \mathcal{N}L\tilde{\Phi}$ and $\mathcal{N}^2 L^2 = \int d\omega_s \int d\omega_i |\Phi(\omega_s, \omega_i)|^2$, where \mathcal{N} is a numerically-calculated normalization constant. Notice that in Eq. (8), $\{\lambda_g\}_{g=1}^{\infty}$ describes the set of eigenvalues with corresponding eigenfunctions $\{f_{s,g}(\omega_s)\}_{g=1}^{\infty}$ and $\{f_{i,g}(\omega_i)\}_{g=1}^{\infty}$.

Thus, by making use of this formalism, we can rewrite the state in Eq. (6) as

$$|\Phi\rangle = \mathcal{N}L \sum_{g=1}^{\infty} \lambda_g \int d\omega_s \int d\omega_i f_{s,g}^*(\omega_s) f_{i,g}^*(\omega_i) \hat{a}_s^\dagger \hat{a}_i^\dagger |\text{vac}\rangle = \mathcal{N} \sum_{g=1}^{\infty} \lambda_g \hat{a}_{s,g}^\dagger \hat{a}_{i,g}^\dagger |\text{vac}\rangle. \quad (9)$$

Note that the signal- (idler-) field creation operators $\hat{a}_{s,g}^\dagger$ ($\hat{a}_{i,g}^\dagger$) of independent Schmidt modes may be related to the spectral ones by writing

$$\hat{a}_s(\omega_s) = \sum_{g=1}^{\infty} f_{s,g}^* (\omega_s) \hat{a}_{s,g}, \quad (10)$$

and similarly for the idler field.

Using the newly introduced operators of the Schmidt modes, the operator $\hat{G}(z)$ can be rewritten as

$$\hat{G}(z) = i\hbar\mathcal{N} \sum_{g=1}^{\infty} \lambda_g \hat{a}_{s,g}^\dagger \hat{a}_{i,g}^\dagger + \text{h.c.} \quad (11)$$

Finally, by using this simplified form of the momentum operator, we can find the evolution of the operators that describe the produced twin beam, i.e. $\hat{a}_{s,g}^\dagger$ and $\hat{a}_{i,g}^\dagger$. To do this, we use the Heisenberg equations with the momentum operator \hat{G} given in Eq. (11), that is,

$$\begin{aligned} \frac{\partial \hat{a}_{s,g}}{\partial z} &= \frac{i}{\hbar} [\hat{G}, \hat{a}_{s,g}] = \lambda_g \mathcal{N} \hat{a}_{i,g}^\dagger, \\ \frac{\partial \hat{a}_{i,g}}{\partial z} &= \frac{i}{\hbar} [\hat{G}, \hat{a}_{i,g}] = \lambda_g \mathcal{N} \hat{a}_{s,g}^\dagger. \end{aligned} \quad (12)$$

Their solution takes the form

$$\begin{aligned} \hat{a}_{s,g}(L) &= u_g \hat{a}_{s,g}(0) + v_g \hat{a}_{i,g}^\dagger(0), \\ \hat{a}_{i,g}(L) &= u_g \hat{a}_{i,g}(0) + v_g \hat{a}_{s,g}^\dagger(0), \end{aligned} \quad (13)$$

where $u_g = \cosh(\mathcal{N}\lambda_g)$ and $v_g = \sinh(\mathcal{N}\lambda_g)$. Notice from Eq. (13) that one can easily determine the number of signal (idler) photons, contained in all modes, by writing

$$N_s = \int d\omega_s \langle \hat{a}_s^\dagger(\omega_s) \hat{a}_s(\omega_s) \rangle = \sum_{g=1}^{\infty} \langle \hat{a}_{s,g}^\dagger \hat{a}_{s,g} \rangle = \sum_{g=1}^{\infty} |v_g|^2, \quad (14)$$

whereas the effective amount of spectral modes, related to the Schmidt number K , is obtained as

$$K_{UV} = \frac{\left(\sum_{g=1}^{\infty} u_g v_g \right)^2}{\sum_{g=1}^{\infty} u_g^2 v_g^2}. \quad (15)$$

Before concluding this section, it is important to remark that although the theoretical model described above is valid for most experimental setups and applications, one must keep in mind that, as any model, it has its limitations; particularly when extremely high photon fluxes are considered [41, 46, 49].

3. INTERACTION OF TWIN BEAMS WITH MATTER

We now consider the interaction of twin beams with an absorbing medium. For the sake of clarity, we assume a simple energy level configuration of the medium where two-photon

transitions occur from a ground (initial) state $|g\rangle$ to a doubly-excited final state $|f\rangle$ via non-resonant intermediate states denoted by $|k\rangle$. For simplicity, we omit any other degree of freedom connected to vibrational spectra of the sample, and assume that the lifetimes of intermediate states are longer than light-matter interaction time. This approximation, which can be satisfied by selecting a proper correlation time between photons [22, 23, 27, 29], implies that effects due to dissipation in the single-excitation manifold (intermediate states) are assumed to be negligible.

The interaction of the electromagnetic field \hat{E} and the sample, in the dipole approximation, can be expressed as

$$\hat{H}(t) = -\hat{d}(t)\hat{E}(t) + \text{h.c.}, \quad (16)$$

where \hat{d} is the dipole-moment operator, whose time evolution is given by

$$\hat{d}(t) = \hat{\mu}_{kg} \exp[i(\varepsilon_k - \varepsilon_g)t] \quad (17)$$

with $\hat{\mu}_{kg}$ being the single-excitation transition amplitude operator from a state $|g\rangle$ (with energy ε_g) to a state $|k\rangle$ (with energy ε_k).

By considering that the medium is initially in its ground state $|g\rangle$, one can make use of second-order time-dependent perturbation theory to find that the resulting TPA signal is given by [28, 29]

$$\begin{aligned} S_{g \rightarrow f} &= \frac{1}{\hbar^4} \int_{-\infty}^{\infty} dt_2 \int_{-\infty}^{t_2} dt_1 \int_{-\infty}^{\infty} dt_2' \int_{-\infty}^{t_2'} dt_1' M^*(t_2, t_1) \\ &\times M(t_2', t_1') \langle \hat{E}^{(-)}(t_2) \hat{E}^{(-)}(t_1) \hat{E}^{(+)}(t_2') \hat{E}^{(+)}(t_1') \rangle, \end{aligned} \quad (18)$$

where $\langle \hat{E}^{(-)}(t_2) \hat{E}^{(-)}(t_1) \hat{E}^{(+)}(t_2') \hat{E}^{(+)}(t_1') \rangle$ corresponds to the four-point correlation function of the optical field. The electric-field operator amplitude is defined as

$$\hat{E}^{(+)}(t) = \hat{E}_s^{(+)}(t) + \hat{E}_i^{(+)}(t), \quad (19)$$

and

$$\begin{aligned} M(t_2, t_1) &= \sum_k \mu_{fk} \mu_{kg} \exp[i(\varepsilon_f - \varepsilon_k)t_2 \\ &+ i(\varepsilon_k - \varepsilon_g)t_1]. \end{aligned} \quad (20)$$

where μ_{fk} denotes the transition dipole moment from the k th intermediate state to the final doubly-excited state $|f\rangle$ and μ_{kg} is defined as in Eq.(17). Notice that the sum over the k states in Eq. (20) appears because the excitation of the medium occurs through non-resonant intermediate states.

Upon substitution of Eq. (19) into Eq. (18), one finds that the TPA signal is composed by sixteen different terms:

$$\begin{aligned}
S_{g \rightarrow f}(\tau_s, \tau_i) &= \frac{1}{\hbar^4} \int_{-\infty}^{\infty} dt_2 \int_{-\infty}^{t_2} dt_1 \int_{-\infty}^{\infty} dt'_2 \int_{-\infty}^{t'_2} dt'_1 M^*(t_2, t_1) M(t'_2, t'_1) \\
&\times \left[\langle \hat{E}_s^{(-)}(t_2) \hat{E}_s^{(-)}(t_1) \hat{E}_s^{(+)}(t'_2) \hat{E}_s^{(+)}(t'_1) \rangle + \langle \hat{E}_s^{(-)}(t_2) \hat{E}_s^{(-)}(t_1) \hat{E}_i^{(+)}(t'_2) \hat{E}_i^{(+)}(t'_1) \rangle \right. \\
&\quad + \langle \hat{E}_s^{(-)}(t_2) \hat{E}_s^{(-)}(t_1) \hat{E}_s^{(+)}(t'_2) \hat{E}_i^{(+)}(t'_1) \rangle + \langle \hat{E}_s^{(-)}(t_2) \hat{E}_s^{(-)}(t_1) \hat{E}_i^{(+)}(t'_2) \hat{E}_s^{(+)}(t'_1) \rangle \\
&\quad + \langle \hat{E}_s^{(-)}(t_2) \hat{E}_i^{(-)}(t_1) \hat{E}_s^{(+)}(t'_2) \hat{E}_s^{(+)}(t'_1) \rangle + \langle \hat{E}_s^{(-)}(t_2) \hat{E}_i^{(-)}(t_1) \hat{E}_s^{(+)}(t'_2) \hat{E}_i^{(+)}(t'_1) \rangle \\
&\quad + \langle \hat{E}_s^{(-)}(t_2) \hat{E}_i^{(-)}(t_1) \hat{E}_i^{(+)}(t'_2) \hat{E}_s^{(+)}(t'_1) \rangle + \langle \hat{E}_s^{(-)}(t_2) \hat{E}_i^{(-)}(t_1) \hat{E}_i^{(+)}(t'_2) \hat{E}_i^{(+)}(t'_1) \rangle \\
&\quad \left. + \{s \leftrightarrow i\} \right] \\
&= I_{ssss} + I_{iiii} + I_{sisi} + I_{siis} + I_{isis} + I_{issi}. \tag{21}
\end{aligned}$$

Notice that we may write the TPA signal as a function of the mutual delay between the beams given by $\tau = (\tau_s - \tau_i)$. This delay can easily be introduced in Eq. (18) by making the substitution $\hat{E}_s(t) \rightarrow \hat{E}_s(t + \tau)$ for the signal field. The symbol $\{s \leftrightarrow i\}$ stands for the contributions that are obtained by interchanging the labels s and i .

Interestingly, one can show that the TPA signal given by Eq. (21) contains only six non-vanishing contributions, corresponding to the terms with even number of indices s, i . These

are collected in the last line of Eq. (21). In the following we will discuss the explicit form of each of these non-vanishing terms.

We start by describing the first two terms, these correspond to the case where photons from a single signal (idler) beam are absorbed. This means that the four-point correlation function describing this process in the signal beam (and similarly in the idler beam) is $\langle \hat{E}_s^{(-)} \hat{E}_s^{(-)} \hat{E}_s^{(+)} \hat{E}_s^{(+)} \rangle$, whose explicit form is given by

$$\begin{aligned}
I_{ssss} &= \frac{1}{\hbar^4} \int_{-\infty}^{\infty} dt_2 \int_{-\infty}^{t_2} dt_1 \int_{-\infty}^{\infty} dt'_2 \int_{-\infty}^{t'_2} dt'_1 M^*(t_2, t_1) M(t'_2, t'_1) \langle \hat{E}_s^{(-)}(t_2) \hat{E}_s^{(-)}(t_1) \hat{E}_s^{(+)}(t'_2) \hat{E}_s^{(+)}(t'_1) \rangle \\
&= \frac{1}{\hbar^2 4\epsilon^2 A^2 c^2 n_s^2} \int_{-\infty}^{\infty} d\omega_s \int_{-\infty}^{\infty} d\omega'_s \mathcal{K}^*(\omega_s) \mathcal{K}(\omega'_s) [F_{1s}(\epsilon_f - \epsilon_g - \omega_s, \omega'_s) F_{1s}(\omega_s, \epsilon_f - \epsilon_g - \omega'_s) + \\
&\quad F_{1s}(\epsilon_f - \epsilon_g - \omega_s, \epsilon_f - \epsilon_g - \omega'_s) F_{1s}(\omega_s, \omega'_s)], \tag{22}
\end{aligned}$$

where the spectral response of the medium is given by the function $\mathcal{K}(\omega)$,

$$\mathcal{K}(\omega) = \sum_k \frac{\mu_{fk} \mu_{kg}}{\epsilon_k - \epsilon_g - \omega}, \tag{23}$$

and the spectral functions of the fields are described by $F_{ij,1s}$. The spectral functions F_{ij} , with $j = i, s$, contain information about the *classical correlations* of the photons and they are given by [50]

$$F_{ij}(\omega, \omega') = \sum_g \sqrt{\omega \omega'} f_{j,g}^*(\omega) f_{j,g}(\omega') |v_g|^2. \tag{24}$$

Note that, as expected, the first two non-vanishing terms of Eq. (21) do not depend on the mutual delay between the signal and idler beams. This implies that these contributions represent a background noise for VSS, as they do not carry spectroscopic information about the sample.

The next contribution, I_{sisi} , may explicitly be written as

$$\begin{aligned}
I_{sisi}(\tau_s, \tau_i) &= \frac{1}{\hbar^4} \int_{-\infty}^{\infty} dt_2 \int_{-\infty}^{t_2} dt_1 \int_{-\infty}^{\infty} dt'_2 \int_{-\infty}^{t'_2} dt'_1 M^*(t_2, t_1) M(t'_2, t'_1) \langle \hat{E}_s^{(-)}(t_2) \hat{E}_i^{(-)}(t_1) \hat{E}_s^{(+)}(t'_2) \hat{E}_i^{(+)}(t'_1) \rangle \\
&= \frac{1}{\hbar^2 4\epsilon^2 A^2 c^2 n_s n_i} \int_{-\infty}^{\infty} d\omega_i \int_{-\infty}^{\infty} d\omega'_i \mathcal{K}^*(\omega_i) \mathcal{K}(\omega'_i) \exp[i(\omega_i - \omega'_i)(\tau_i - \tau_s)] \\
&\quad \times [F_{2i}^*(\epsilon_f - \epsilon_g - \omega_i, \omega_i) F_{2i}(\epsilon_f - \epsilon_g - \omega'_i, \omega'_i) + F_{1i}(\omega_i, \omega'_i) F_{1s}(\epsilon_f - \epsilon_g - \omega_i, \epsilon_f - \epsilon_g - \omega'_i)]. \tag{25}
\end{aligned}$$

Notably, this term contains the function F_2 , which is directly related to the *quantum correlations* between the fields and is defined by [50]

$$F_2(\omega, \omega') = \sum_g \sqrt{\omega \omega'} f_{s,g}(\omega) f_{i,g}(\omega') v_g u_g. \quad (26)$$

$$\begin{aligned} I_{\text{siis}}(\tau_s, \tau_i) &= \frac{1}{\hbar^4} \int_{-\infty}^{\infty} dt_2 \int_{-\infty}^{t_2} dt_1 \int_{-\infty}^{\infty} dt_2' \int_{-\infty}^{t_2'} dt_1' M^*(t_2, t_1) M(t_2', t_1') \langle \hat{E}_s^{(-)}(t_2) \hat{E}_i^{(-)}(t_1) \hat{E}_i^{(+)}(t_2') \hat{E}_s^{(+)}(t_1') \rangle \\ &= \frac{1}{\hbar^2 4\epsilon^2 A^2 c^2 n_s n_i} \int_{-\infty}^{\infty} d\omega_i \int_{-\infty}^{\infty} d\omega_s \mathcal{K}^*(\omega_i) \mathcal{K}(\omega_s) \exp[i(\omega_i + \omega_s)(\tau_i - \tau_s) + i(\epsilon_f - \epsilon_g)(\tau_s - \tau_i)] \\ &\quad \times [F_2^*(\epsilon_f - \epsilon_g - \omega_i, \omega_i) F_2(\omega_s, \epsilon_f - \epsilon_g - \omega_s) + F_{1s}(\epsilon_f - \epsilon_g - \omega_i, \omega_s) F_{1i}(\omega_i, \epsilon_f - \epsilon_g - \omega_s)]. \end{aligned} \quad (27)$$

The remaining terms are easily obtained by interchanging the label s and i in Eqs. (25) and (27), respectively.

4. VIRTUAL-STATE SPECTROSCOPY WITH ENTANGLED BEAMS

We are now ready to discuss the implementation of the VSS protocol with intense twin beams. For this, we consider a simple model system in which the two-photon excitation energy of the medium $|g\rangle \rightarrow |f\rangle$ corresponds to the pump wavelength $\lambda_{p0} = 400$ nm ($E_f = 3.1$ eV considering $\epsilon_g = 0$ eV). The intermediate-level energies are randomly chosen to be $\epsilon_k = (\epsilon_f + \{0.05, 0.075, 0.089\}) / 2$ eV. Following this energy-level configuration, we consider a nonlinear crystal producing degenerate photon pairs with a wavelength of 800 nm. Notice that the central frequency of the down-converted photons does not match any of the intermediate states, thus making them effectively non-resonant (or virtual) transitions. Moreover, the energies of these transitions, although random, are kept close to the central frequency of the photons. The reason for this lies in the fact that entangled two-photon absorption is optimal un-

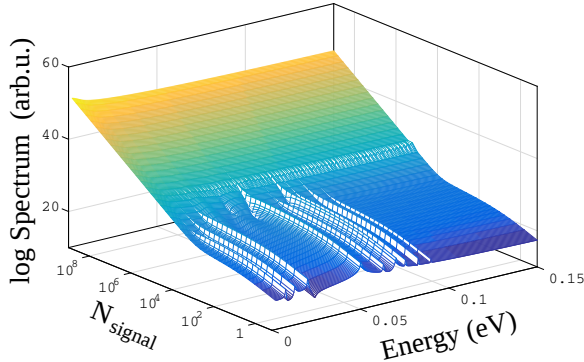


Fig. 2. TPA spectrogram as a function of the number N_{signal} of photons in the twin beam; the delay range considered is $0 \leq \tau \leq 8$ ps, the length of the nonlinear crystal is $L = 1$ mm and the pump pulse duration is set to $\tau_p = 1$ ps, and the inverse group velocities are set to $G_s = 5.2$ ps/m and $G_i = 5.6$ ps/m. For the sake of simplicity, the energy axis is defined by means of the energy mismatch: $2\epsilon_k - \epsilon_f$.

The fourth term, I_{siis} , is equal to the cross correlation (si) – (is). Here, it is important to highlight the fact that (si) and (is) are not mutually interchangeable as time-ordering must be satisfied. Consequently, this term writes

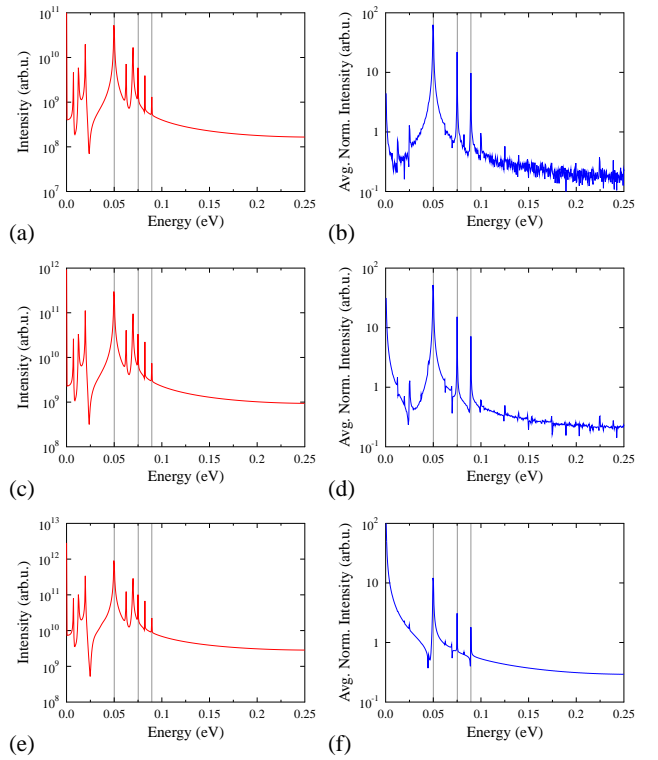


Fig. 3. TPA spectrograms, and their corresponding average, for twin beams carrying (a,b) $N_s = 1$, (c,d) $N_s = 10$, and (e,f) $N_s = 100$ photons. Average was performed over and ensemble of 100 crystals of different lengths $L \in \{20, 22\}$ mm. The vertical grey lines indicate the relative energies, $2\epsilon_k - \epsilon_f$, of the intermediate levels.

der conditions of near-resonance between entangled photons and the intermediate states [51]. Finally, we assume the group velocity matching condition [52]: $G_p = (G_s + G_i)/2$, with G_s , G_i and G_p being in turn the inverse group velocities of the signal, idler and pump beams. We have considered this condition because it allows for a simple interpretation and control of the correlations between the photon beams.

Figure 2 shows the TPA spectrogram — Fourier transform w.r.t. the delay between beams, of the TPA signal — as a func-

tion of the number of photons $N_{\text{signal}} \equiv N_s = N_i$ carried by the twin beam. We can immediately see from Fig. 2 that several peaks emerge from the Fourier transform of the TPA signal. These peaks appear as a result of the interference between different pathways through which two-photon excitation of the medium can occur [27, 29]. Concurrently, as pointed out previously [53], we can see that the visibility of the TPA signal is affected as the number of photons N_{signal} is increased, thus defining a limit in the photon flux at which VSS can be implemented. Interestingly, one can make use of the signal shown in Fig. 2 to extract information related to the energy level structure of the medium [27–29]. To do so, we perform an average of the normalized TPA spectrograms over different crystal lengths,

$$\bar{S}_{g \rightarrow f}(\tau) = \frac{1}{N} \sum_{n=1}^N \frac{S_{g \rightarrow f}(\tau; L_n)}{\max \{S_{g \rightarrow f}(\tau; L_n)\}}, \quad (28)$$

where N is the number of crystal lengths used to obtain the corresponding TPA signals. Notice that by changing the crystal length, one effectively modifies the correlation (entanglement) time between photons [27–29], which means that the average is effectively performed over different correlation times. Therefore, we can experimentally obtain the average of the TPA signals by using different strategies, depending on the configuration of the setup that is being used. For instance, in type-I SPDC, changing the width of the pump beam modifies the correlation between photons [54], whereas in type-II, the configuration used in this work, the correlation time is linearly proportional to the crystal length [55], so a proper set of two wedge-shaped nonlinear/compensation crystals might be used. Another alternative to control the correlation time of the photons is by introducing frequency chirps in either the pump pulse or down-converted beams [53], or by changing the time duration of the pump, as depicted in Fig. 4.

Figure 3 shows the TPA spectrograms, and their corresponding average over 100 crystal lengths, for twin beams carrying (a,b) $N_s = 1$, (c,d) $N_s = 10$, and (e,f) $N_s = 100$ photons. Notice that by averaging the TPA spectrograms only three peaks remain in the signal, whose locations reveal the energy of the intermediate states that contribute to the two-photon excitation of the medium. Interestingly, the results in Figs. 2 and 3 show that although VSS can be implemented with entangled fields carrying a large number of photons, there exists a threshold in the photon-pair number, as the height of the peaks with respect to the background noise (signal-to-noise ratio) gets diminished with increasingly larger photon fluxes. It is important to remark that in obtaining the results shown in Fig. 3, we have assumed that the temporal walk-off of the photons is much shorter than the lifetime of the intermediate levels.

To explore the limits on the photon flux that can be used in the implementation of VSS, we now analyze the terms that contribute to the overall TPA signal. For the sake of simplicity, we divide all terms into three different groups. The first group (I_{noise}) contains the terms that are independent of the delay between the beams, namely the first two terms of Eq. (21). As we discussed above, these terms do not contain spectroscopic information and represent a background noise of the TPA signal. The second group (I_{class}) contains the terms related to the classical correlations, represented by those containing products of the functions F_{1j} , with $j = s, i$ [see Eqs. (25) and (27)]. Notice that these functions contain single-beam correlations only. Finally, the third group (I_{quant}), which depends on products of the functions F_2 , represents the quantum correlations between

the two photon fields. This final group is the most important one, as it contains the information about the intermediate-state transitions occurring during the TPA process.

Figure 4 shows the delay-integrated TPA contributions, considering three different initial states, namely spectrally (a,b) anti-correlated, (c,d) quasi uncorrelated, and (e,f) correlated photons. The delay-integrated signals are obtained by integrating the TPA signal [Eq. (21)] over a delay interval $\Delta\tau$, while fixing the correlation time between photons by means of the pump-pulse duration τ_p . Notice that the delay-integrated signals with varying frequency correlations [depicted in Figs. 4(b,d,f)] reflect the mutual interplay between all participating terms (noise, classical, and quantum). More importantly, they show that quantum contributions (blue solid line), where spectroscopic information about the sample resides, dominates in a low-to-moderate photon flux regime for anti-correlated and quasi uncorrelated photons. This effect can be understood in terms of the Schmidt modes of the two-photon state [depicted in Figs. 4(b,d)]. As the number of photons is increased, the number of effectively populated Schmidt modes becomes smaller. The reduction of populated Schmidt modes results in a reduced spectral overlap between the absorbed entangled photons and the sample under study, thus lowering the spectroscopic resolution of the system.

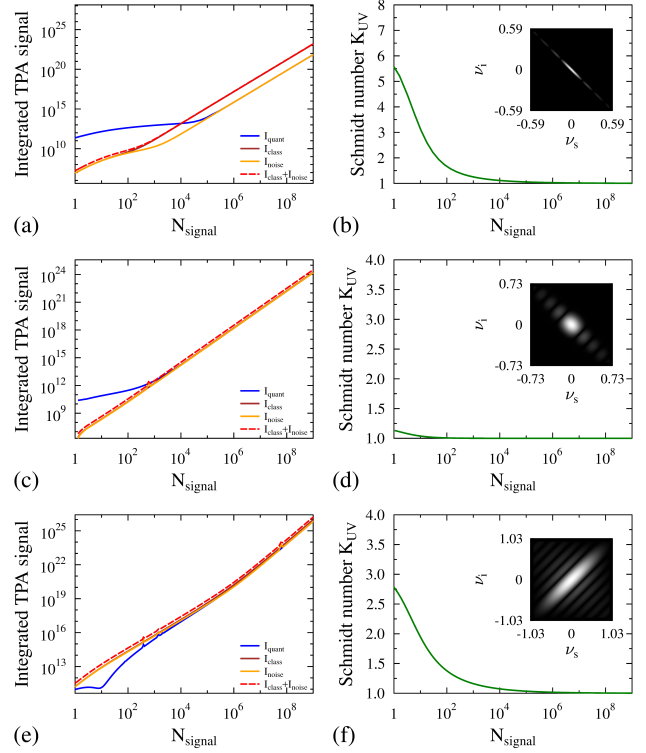


Fig. 4. Delay-integrated TPA signal (left column) for spectrally (a) anti-correlated, (c) uncorrelated, and (e) correlated two-photon states, and their corresponding Schmidt decomposition (right column). The symbols $\nu_{s,i} = \omega_{s,i} - \omega_{s,i}^0$ stand for the frequency deviations from the central frequency $\omega_{s,i}^0$ of the photon fields. Integration of the signals was performed over a delay range $\Delta\tau$ of $0 \leq \tau \leq 8$ ps. The length of the nonlinear crystal is $L = 1$ mm, and the pump pulse duration was set to (a) $\tau_p = 20$ fs, (c) $\tau_p = 110$ fs, and (e) $\tau_p = 1$ ps.

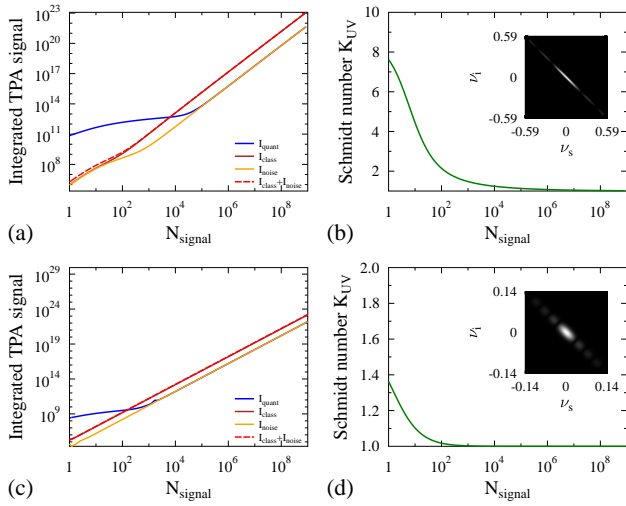


Fig. 5. Delay-integrated TPA signal (left column) for the fixed pump-duration $\tau_p = 1$ ps for different values of the crystal length (a) $L=0.75$ mm and (c) $L=5$ mm with the corresponding Schmidt numbers (right column) plotted in (b) and (d). Integration of the signals was performed over a delay range $\Delta\tau$ of $0 \leq \tau \leq 8$ ps.

Remarkably, when correlated photons interact with the sample, we find that the signal carrying useful information is completely suppressed. This demonstrates the fact that entanglement alone is not the key ingredient for implementing VSS, but rather a combination of entanglement and anti-correlation of the absorbed photons [29]. In particular, for our model system, the use of spectrally anti-correlated photons guarantees that the transition from the quantum (linear) to the classical (quadratic) regime occurs around $N_{\text{signal}} \approx 10^4$ signal photons. It is important to remark that this photon-number limit is valid for the model system considered here. As we discussed above, this limit strongly depends on the number of Schmidt modes contained in the photon spectra. Indeed, as shown in Fig. 5, a broader spectrum of anti-correlated photons will push the limit towards higher values of photon numbers, whereas a narrower spectrum will reduce the photon flux at which VSS can be successfully implemented.

Finally, notice that the Schmidt number K_{UV} is inversely related to the length of crystal L , as depicted in Fig. 5. From here we can see that the use of shorter lengths of the crystal produces a broader spectrum, with rich spatial structure, in the produced photon fields. This shows the many knobs that non-classical light provides to emerging nonlinear spectroscopy techniques.

5. CONCLUSIONS

We have presented a thorough analysis of the virtual-state spectroscopy technique implemented with intense twin beams. We showed that the virtual-state spectroscopy may be implemented with entangled twin beams carrying up to 10^4 photon pairs, provided that a proper configuration of the experimental setup and a particular shape of the spectral correlations between photons is selected. Our results suggest that by making use of intense twin beams one might be able to detect two-photon absorption signals up to four orders of magnitude larger

than previously reported, thus paving the way towards the first experimental implementation of the virtual-state spectroscopy technique.

ACKNOWLEDGMENT

JS thanks Alejandra Catalina Valencia González and Mayerlin Nuñez Portela for useful and stimulating discussions. JS also acknowledges the Faculty of Science of Universidad de los Andes. This work was supported by projects 17-23005Y (JS) and 15-08971S (JP) of the Czech Science Foundation, and project LO1305 of MŠMT ČR. RJLM gratefully acknowledge financial support from DGAPA-UNAM, Mexico, under the project UNAM-PAPIIT IA100718.

REFERENCES

1. Y. Shen, *Principles of Nonlinear Optics* (Wiley-Interscience, New York, 1984).
2. S. Mukamel, *Principles of Nonlinear Optical Spectroscopy*, Oxford series in optical and imaging sciences (Oxford University Press, Oxford, 1999).
3. B. Dayan, A. Pe'er, A. A. Friesem, and Y. Silberberg, "Two photon absorption and coherent control with broadband down-converted light," *Phys. Rev. Lett.* **93**, 023005 (2004).
4. J. Kojima and Q.-V. Nguyen, "Entangled biphoton virtual-state spectroscopy of the $A^2\Sigma^+ - X^2\Pi$ system of OH," *Chem. Phys. Lett.* **396**, 323 (2004).
5. D.-I. Lee and T. Goodson III, "Entangled photon absorption in an organic porphyrin dendrimer," *J. Phys. Chem. B* **110**, 25582–25585 (2006).
6. O. Roslyak and S. Mukamel, "Multidimensional pump-probe spectroscopy with entangled twin-photon states," *Phys. Rev. A* **79**, 063409 (2009).
7. A. R. Guzman, M. R. Harpham, O. Süber, M. M. Haley, and T. Goodson III, "Spatial control of entangled two-photon absorption with organic chromophores," *J. Am. Chem. Soc.* **132**, 7840–7841 (2010).
8. H. Oka, "Efficient selective two-photon excitation by tailored quantum-correlated photons," *Phys. Rev. A* **81**, 063819 (2010).
9. H. Oka, "Selective two-photon excitation of a vibronic state by correlated photons," *J. Chem. Phys.* **134**, 124313 (2011).
10. H. Oka, "Control of vibronic excitation using quantum-correlated photons," *J. Chem. Phys.* **135**, 164304 (2011).
11. L. J. Salazar, D. A. Guzmán, F. J. Rodríguez, and L. Quiroga, "Quantum-correlated two-photon transitions to excitons in semiconductor quantum wells," *Opt. Express* **20**, 4470 (2012).
12. F. Schlawin, K. E. Dorfman, B. P. Fingerhut, and S. Mukamel, "Manipulation of two-photon-induced fluorescence spectra of chromophore aggregates with entangled photons: A simulation study," *Phys. Rev. A* **86**, 023851 (2012).
13. M. G. Raymer, A. H. Marcus, J. R. Widom, and D. L. P. Vitulo, "Entangled photon-pair two-dimensional fluorescence spectroscopy (EPP-2DFS)," *J. Phys. Chem. B* **117**, 15559–15575 (2013).
14. D. A. Kalashnikov, Z. Pan, A. I. Kuznetsov, and L. A. Krivitsky, "Quantum spectroscopy of plasmonic nanostructures," *Phys. Rev. X* **4**, 011049 (2014).
15. K. E. Dorfman, F. Schlawin, and S. Mukamel, "Nonlinear optical signals and spectroscopy with quantum light," *Rev. Mod. Phys.* **88**, 045008 (2016).
16. D. A. Kalashnikov, E. V. Melik-Gaykazyan, A. A. Kalachev, Y. F. Yu, A. I. Kuznetsov, and L. A. Krivitsky, "Time-resolved spectroscopy with entangled photons," arXiv preprint arXiv:1608.07326 (2016).
17. F. Schlawin, "Entangled photon spectroscopy," *J. Phys. B* **50**, 203001 (2017).
18. J. P. Villabona-Monsalve, O. Calderón-Losada, M. N. Portela, and A. Valencia, "Entangled two photon absorption cross section on the 808 nm region for the common dyes zinc tetraphenylporphyrin and rhodamine b," *J. Phys. Chem. A* **121**, 7869 (2017).

19. O. Varnavski, B. Pinsky, and T. Goodson III, "Entangled photon excited fluorescence in organic materials: an ultrafast coincidence detector," *J. Phys. Chem. Lett.* **8**, 388 (2017).
20. F. Schlawin and A. Buchleitner, "Theory of coherent control with quantum light," *New J. Phys.* **19**, 013009 (2017).
21. J. Javanainen and P. L. Gould, "Linear intensity dependence of a two-photon transition rate," *Phys. Rev. A* **41**, 5088–5091 (1990).
22. H.-B. Fei, B. M. Jost, S. Popescu, B. E. A. Saleh, and M. C. Teich, "Entanglement-induced two-photon transparency," *Phys. Rev. Lett.* **78**, 1679 (1997).
23. F. Schlawin, K. E. Dorfman, B. P. Fingerhut, and S. Mukamel, "Suppression of population transport and control of exciton distributions by entangled photons," *Nat. Commun.* **4**, 1782 (2013).
24. M. Shapiro and P. Brumer, "Generation and control of chains of entangled atom-ion pairs with quantum light," *Phys. Rev. Lett.* **106**, 150501 (2011).
25. M. Shapiro and P. Brumer, *Quantum control of molecular processes* (Wiley-VCH, Weinheim, 2012).
26. J. Perina, *Quantum statistics of linear and nonlinear optical phenomena* (Kluwer, Boston, 1991).
27. B. E. A. Saleh, B. M. Jost, H.-B. Fei, and M. C. Teich, "Entangled-photon virtual-state spectroscopy," *Phys. Rev. Lett.* **80**, 3483 (1998).
28. J. Peřina, B. E. A. Saleh, and M. C. Teich, "Multiphoton absorption cross section and virtual-state spectroscopy for the entangled n-photon state," *Phys. Rev. A* **57**, 3972 (1998).
29. R. de J. Le3n-Montiel, J. Svozilik, L. J. Salazar-Serrano, and J. P. Torres, "Role of the spectral shape of quantum correlations in two-photon virtual-state spectroscopy," *New J. Phys.* **15**, 053023 (2013).
30. B. W. Shore, "Definition of virtual levels," *Am. J. Phys.* **47**, 262 (1979).
31. J. J. Sakurai, *Modern Quantum Mechanics* (MA: Addison-Wesley, Boston, 1994).
32. E. Brambilla, A. Gatti, M. Bache, and L. A. Lugiato, "Simultaneous near-field and far-field spatial quantum correlations in the high-gain regime of parametric down-conversion," *Phys. Rev. A* **69**, 023802 (2004).
33. O. Jedrkiewicz, Y. K. Jiang, E. Brambilla, A. Gatti, M. Bache, L. A. Lugiato, and P. Di Trapani, "Detection of sub-shot-noise spatial correlation in high-gain parametric down-conversion," *Phys. Rev. Lett.* **93**, 243601 (2004).
34. M. Bondani, A. Allevi, G. Zambra, M. G. A. Paris, and A. Andreoni, "Sub-shot-noise photon-number correlation in a mesoscopic twin beam of light," *Phys. Rev. A* **76**, 013833 (2007).
35. J.-L. Blanchet, F. Devaux, L. Furfaro, and E. Lantz, "Measurement of sub-shot-noise correlations of spatial fluctuations in the photon-counting regime," *Phys. Rev. Lett.* **101**, 233604 (2008).
36. B. Dayan, A. Pe'er, A. A. Friesem, and Y. Silberberg, "Nonlinear interactions with an ultrahigh flux of broadband entangled photons," *Phys. Rev. Lett.* **94**, 043602 (2005).
37. R. Shimizu and K. Edamatsu, "High-flux and broadband biphoton sources with controlled frequency entanglement," *Optics Express* **17**, 16385 (2009).
38. F. Schlawin and S. Mukamel, "Photon statistics of intense entangled photon pulses," *J. Phys. B: At. Mol. Opt. Phys.* **46**, 175502 (2013).
39. J. Peřina Jr., "Coherence and mode decomposition of intense twin beams," *Phys. Rev. A* **92**, 013833 (2015).
40. J. Peřina Jr., "Spatial, spectral and temporal coherence of ultra-intense twin beams," *Phys. Rev. A* **93**, 013852 (2016).
41. J. Peřina Jr., O. Haderka, A. Allevi, and M. Bondani, "Internal dynamics of intense twin beams and their coherence," *Sci. Rep.* **6**, 22320 (2016).
42. W. Wasilewski, A. I. Lvovsky, K. Banaszek, and C. Radzewicz, "Pulsed squeezed light: Simultaneous squeezing of multiple modes," *Phys. Rev. A* **73**, 063819 (2006).
43. C. J. McKinstrie, "Unitary and singular value decompositions of parametric processes in fibers," *Opt. Commun.* **282**, 583 (2009).
44. C. J. McKinstrie and M. Karlsson, "Schmidt decompositions of parametric processes I: Basic theory and simple examples," *Opt. Express* **21**, 1374–1394 (2013).
45. A. Christ, K. Laiho, A. Eckstein, K. N. Cassemiro, and C. Silberhorn, "Probing multimode squeezing with correlation functions," *New J. Phys.* **13**, 033027 (2011).
46. A. Christ, B. Brecht, W. Mauerer, and C. Silberhorn, "Theory of quantum frequency conversion and type-II parametric down-conversion in the high-gain regime," *New J. Phys.* **15**, 053038 (2013).
47. C. K. Law, I. A. Walmsley, and J. H. Eberly, "Continuous frequency entanglement: Effective finite hilbert space and entropy control," *Phys. Rev. Lett.* **84**, 5304–5307 (2000).
48. C. K. Law and J. H. Eberly, "Analysis and interpretation of high transverse entanglement in optical parametric down conversion," *Phys. Rev. Lett.* **92**, 127903 (2004).
49. A. M. P3rez, T. S. Iskhakov, P. Sharapova, S. Lemieux, O. V. Tikhonova, M. V. Chekhova, and G. Leuchs, "Bright squeezed-vacuum source with 1.1 spatial mode," *Opt. Lett.* **39**, 2403–2406 (2014).
50. V. Torres-Company, A. Valencia, M. Hendrych, and J. P. Torres, "Cancellation of dispersion and temporal modulation with nonentangled frequency-correlated photons," *Phys. Rev. A* **83**, 023824 (2011).
51. L. Upton, M. Harpham, O. Suzer, M. Richter, S. Mukamel, and T. Goodson III, "Optically excited entangled states in organic molecules illuminate the dark," *J. Phys. Chem. Lett.* **4**, 2046 (2013).
52. T. E. Keller and M. H. Rubin, "Theory of two-photon entanglement for spontaneous parametric down-conversion driven by a narrow pump pulse," *Phys. Rev. A* **56**, 1534 (1997).
53. J. Svozilik, J. Peřina Jr, and R. de J. Le3n-Montiel, "Practical entangled-photon virtual-state spectroscopy using intense twin beams," *arXiv preprint arXiv:1608.07326* (2016).
54. A. Joobeur, B. E. A. Saleh, and M. C. Teich, "Spatiotemporal coherence properties of entangled light beams generated by parametric down-conversion," *Phys. Rev. A* **50**, 3349 (1994).
55. Y. H. Shih and A. V. Sergienko, "A two-photon interference experiment using type ii optical parametric down conversion," *Phys. Lett. A* **191**, 201 (1994).